RSC Applied Polymers

ROYAL SOCIETY OF CHEMISTRY

PAPER

View Article Online
View Journal

Cite this: DOI: 10.1039/d6lp00013d

Unexpected crystallization barrier in partially miscible polymer blends – a new opportunity for tailoring self-reinforcing polymer materials

Robert D. L. Jerusalem, Michail Maricanov, Anas Kerkour el Miad, Hannah Keune, Frank Katzenberg and Joerg C. Tiller *

Polymers that can store mechanical energy administered shock-wise would be superior to simply shock absorbing elastic materials due to advanced safety and the ability to simultaneously store energy. A way to obtain such novel material properties is to design a polymeric system that is rubber-elastic and has the ability to form shape-stabilizing crystals upon strain while no such crystals are formed upon thermal crystallization. So far no such material exists. This study investigates, if cross-link partially miscible blends composed of semi-crystalline poly(vinylidene fluoride) (PVDF) and amorphous poly(2-ethyl-2-oxazoline) (PEtOx) shows such behavior. Networks with a PVDF content of 65 wt% were found to inhibit the thermal crystallization of PVDF at ambient temperature by 69% of the maximal degree of crystallinity. Rapid stretching this material affords a strain-induced crystallization, which results in self-inforcement and stabilization of the stretched shape. The crystallization within these networks is inhibited even above the glass transition temperature (T_g) of the blends. This unusual behavior is attributed to a local compositional segregation during formation of a minor fraction of seed crystals, which increases the local T_g in the amorphous interphase between crystals and mixed amorphous blend that retains the lower mixture T_g. The unexpected effect prevents further crystal growth even in a material with an overall T_g below ambient temperature. The increased local T_g is increasing the stiffness of the material, making it unsuitable as shock absorber, but the blend approach is a promising way towards rapid energy and shock absorbing materials.

Received 16th January 2026,
Accepted 23rd March 2026

DOI: 10.1039/d6lp00013d

rsc.li/rscapplpolym

Introduction

Materials that can adapt their properties in response to changing environmental conditions are referred to as *adaptive materials*.[1–4] Of particular interest are adaptive materials that respond to an external stimulus such as solvents,[5–7] salt concentration,[8] pH,[9] electromagnetic radiation[10–12] or mechanical stress[13–15] with a change in their mechanical properties, such as the Young's modulus, in order to absorb shocks. Although several materials with shock-absorbing properties are known, they all have the disadvantage that the mechanical energy administered to them must either be fully dissipated by plastic deformation or be released as vibrations. In the case of mechanical failure of elastic materials, the energy is released as a dangerous, rapid backslash. This means that plastically deforming shock-absorbing materials are damaged after the shock, while elastic shock-absorbing materials are inconvenient due to ongoing vibrations, and can be very dangerous in the event of mechanical failure. An ideal shock-absorbing material would be able to absorb a shock and rapidly store the deformation energy to avoid vibrations or dangerous rebound. Currently, no technical material capable of this behaviour exists. One possibility to achieve this behaviour would be an amorphous rubber-elastic polymeric material that undergoes strain-induced crystallisation during rapid stretching, with the formed crystals stabilising the stretched shape. We call such a material a rapid energy and shock absorbing (RESA) material, and it would be safer than common shock absorbers and can be easily regenerated.

Natural rubber (NR) is the oldest and most widely used representative of shock absorbing materials, as it transforms from a rubber-elastic to an energy-elastic material when stretched. The underlying mechanism is strain-induced crystallization, which enables natural rubber to withstand very high loads even at large deformations. When NR is unloaded, the strain-induced crystals typically melt, and the rubber returns to its original state. This makes natural rubber ideally suited

Biomaterials & Polymer Science, Department of Biochemical and Chemical Engineering, TU Dortmund, 44221 Dortmund, Germany.
E-mail: joerg.tiller@tu-dortmund.de

for reversibly absorbing shock-like loads, such as those occurring during a bungee jump. In order to prevent the melting of strain-induced crystals, thereby stabilizing the material in its stretched, highly oriented state and fully absorbing the deformation energy, NR was rendered into a highly efficient shape-memory polymer.[16,17] However, the crystallization of NR requires several seconds before the stretched state becomes fully stabilized and the energy applied during deformation is permanently stored. Therefore, SMNR is not a RESA material.[18] A natural material that is to some extent capable of absorbing shock and partially storing deformation energy upon formation of stable strain induced crystals is spider silk.[19] The general feasibility of using a synthetic strain-induced crystallizing polymer as a RESA material was demonstrated with crosslinked syndiotactic polypropylene (x-sPP).[18] Once brought to the amorphous state by quenching, this material can crystallize with a sufficiently fast rate upon stretching to make it suitable as shock- and energy-absorbing material, *e.g.*, as safety rope. Unfortunately, x-sPP is not stable in the amorphous state at room temperature, since thermal crystallization occurs within less than 5 min[18] and leads to a complete loss of its shock- and energy-absorbing capabilities.

Since all attempts in unpublished preliminary studies to prevent thermal crystallization, for example by adding white oil, have failed, this work pursues a new strategy to obtain a mostly amorphous, rubber-elastic material that crystallizes and, thus, self-reinforces only when stretched. The idea is to crosslink a partially miscible blend of a semi-crystalline low-T_g and an amorphous high-T_g component that can be quenched into an amorphous rubber elastic state. The question is whether the crosslinking along with the partial miscibility allows for retaining the amorphous state in relaxed form, but enables strain-induced crystallization by mechanically induced separation of the polymer chains.

Poly(vinylidene fluoride) (PVDF), a semi-crystalline fluoropolymer with a T_g of about −40 °C is a promising candidate for testing our strategy to realize a rubber elastic, deformable material that self-reinforces when stretched upon strain-induced crystallization, since it offers a significant miscibility with numerous carbonyl-group containing polymers due to strong dipolar interactions.[20–23] Due to a T_g of about 54 °C and a miscibility with up to 30 wt% PVDF, poly(2-ethyl-2-oxazoline) (PEtOx) was chosen to be blended with PVDF in this work.[24] In previous work, we could show that such crosslinked blends can act as heating rate sensitive shape memory materials.[25]

This study investigates, how crosslinked blends of PVDF and PEtOx behave after being quenched into an amorphous state with respect to composition dependent thermal crystallization, strain-induced crystallization, and resulting mechanical properties.

Experimental

Materials

All materials were used without further purification. Poly(vinylidene fluoride) (PVDF) (Solef 1008, M_n = 61 kg mol^{-1}, $Đ$ = 1.8) was kindly provided by Solvay SA. Poly(2-ethyl-2-oxazoline) (PEtOx) with a molecular weight labeled as 500 kg mol^{-1} was obtained from Alfa Aesar, Inc. Dimethyl sulfoxide (DMSO, 99% purity) was obtained from Fisher Scientific, Inc. and dicumyl peroxide (DCP, 98% purity) and triallyl isocyanurate (TAIC, 98% purity) were purchased from Acros Organics, Inc.

Blend preparation

PVDF/PEtOx blends were prepared by melt mixing 5 g PVDF and PEtOx (*m*PVDF + *m*PEtOx), across the entire concentration range, in a twin-screw extruder (HAAKE MiniLab 3 Micro-Compounder, Thermo Fisher Scientific, Inc.) for 5 min at a temperature of 180 °C using a screw speed of 60 rpm. The extrudate was subsequently pelletized and compression moulded at a temperature of 180 °C to 0.5 mm thick sheets using steel spacers in a heating press (Paul-Otto-Weber Maschinen- & Apparatebau GmbH). The amounts of ingredients used in the blend preparation can be found in Table S1 of the SI.

Network synthesis

Differently composed PVDF/PEtOx blends were radically crosslinked with DCP as thermal initiator and TAIC as crosslinker in a ratio of 1 : 8, according to previously published work.[25] To this end, the respective PVDF and PEtOx amounts (m_{PVDF} + m_{PEtOx} = 5 g) were dissolved in 25 ml dimethyl sulfoxide (DMSO) in a glass Petri dish on a hot plate set to a temperature of 100 °C. The mixture was stirred at the heating plate until the polymer/DMSO weight ratio reaches 1 : 1 (wt/wt) detected by frequent weighing. Subsequently, 0.1 g DCP and 0.8 g TAIC were added for synthesis of lowly crosslinked networks and again thoroughly stirred. 0.25 g DCP and 2 g TAIC were added for synthesis of the highly crosslinked networks. In the following lowly and highly crosslinked networks are referred to as LC and HC, respectively. The compositions of the mixtures of components used for PVDF/PEtOx LC and HC network synthesis are listed in Tables S2 and S3 in the SI. Steel spacers with a thickness of 0.5 mm were used to compression mould sheets using a heating press (Paul-Otto-Weber Maschinen- & Apparatebau GmbH) at a temperature of 160 °C. Curing was carried out in the heating press at the same temperature for 30 min. The networks were then dried in a vacuum oven at a pressure of 30 mbar and a temperature of 120 °C for at least 4 h (Scheme 1).

Thermal analysis

The netchain molecular weights M_c of selected compositions were calculated from the storage modulus G' taken at a temperature of 200 °C determined in a Dynamical Mechanical Analyzer (DMA 850, TA Instruments Inc.). Square samples with dimensions (l × b) of 10 × 10 mm^2 were cut, mounted in a shear sandwich clamp and measured between 180 and 220 °C at a heating rate of 5 K min^{-1}. The M_cs were determined as per Flory's theory of viscoelasticity using eqn (1).

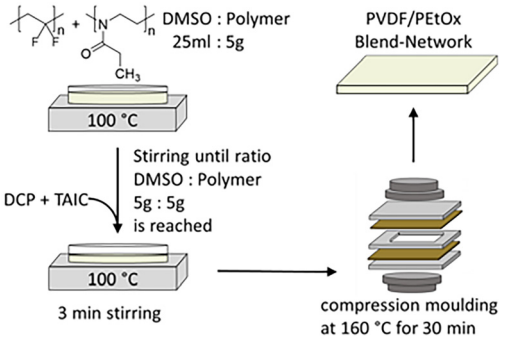

Scheme 1 Scheme illustrating the network synthesis of PVDF/PEtOx blend networks.

$$M_c = \frac{\rho(T,w)\cdot R\cdot T}{G'(T)} \quad (1)$$

$G'(T)$ denotes the storage modulus, R is the universal gas constant (8.314 J (mol K)$^{-1}$), and T is the absolute temperature. The weight average density $\rho(T,w)$ at 200 °C was determined for PVDF according to reference[26] to ρ_{PVDF} = 1.475 g cm^{-3} and for PEtOx, the density was calculated using the thermal expansion coefficient in accordance with reference[27] to ρ_{PEtOx} = 0.972 g cm^{-3}.

The glass transition temperature T_g, melting temperature T_m, crystallization temperature T_c and the respective enthalpies ΔH_m an ΔH_c were determined with a Differential Scanning Calorimeter (DSC) (DSC 2910, TA Instruments, Inc.) using a heating rate of 10 K min^{-1}. The total crystallinity was calculated as the ratio of melting enthalpy ΔH_m and the heat of fusion ΔH_m° (eqn (2)). The crystallinity of the samples x_c after quenching sealed inside a Teflon bag in ice water or defined cooling with 10 K min^{-1} was determined analogously by relating the difference of the melting enthalpy ΔH_m and the cold crystallization enthalpy ΔH_{cc} to the heat of fusion ΔH_m° of PVDF-crystals, which is assumed to be 105 J g^{-1}.[28]

$$x_c = \frac{\Delta H_m - \Delta H_{cc}}{\Delta H_m^\circ} \quad (2)$$

Because of strong intermolecular forces between PVDF and PEtOx chains, the mixture glass transition temperatures $T_{g,calc}$ were calculated according to Utraki (eqn (3)).[29] The interaction parameter K^* was determined by fitting the calculated $T_{g,calc}$ to the measured T_g of fully miscible compositions, for the blends and the two differently crosslinked blend networks.

$$T_{g,calc} = (1 + K^* w_{PEtOx} w_{PVDF})\left[w_{PEtOx} T_{g,PEtOx}^{3/2} + w_{PVDF} T_{g,PVDF}^{3/2}\right]^{2/3} \quad (3)$$

The T_g of selected compositions were also measured using a Dynamic Mechanical Analyzer (DMA) (DMA 850, TA Instruments, Inc.). To this end, samples with a cross section of 0.5 × 10 mm^2 and *ca.* 20 mm length were prepared, mounted to the film-tension clamp and analysed with a heating rate of 10 K min^{-1}, a frequency of 1 Hz, an amplitude of 20 μm and a preload force of 0.01 N.

Microstructural characterisation

Wide-angle X-ray-scattering (WAXS) was carried out at a Bruker Nanostar (Bruker AXS GmbH) utilizing a heated stage to gain information about crystallization at different temperatures and times after quenching. A micro-focus X-ray source (IμS, Incoatec GmbH) with a Cu-anode and integrated Montel Optic was operated at 50 kV and 600 mA to emit X-rays with a wavelength of 0.15406 nm. WAXS patterns were recorded for 900 s with a sample-to-detector distance of 12.04 mm on a VANTEC-2000 detector (Bruker AXS GmbH). PVDF unit cell parameters of α-phase and β-phase are a = 0.496 nm, b = 0.964 nm, c = 0.462 nm and a = 0.858 nm, b = 0.491 nm, and c = 0.256 nm, respectively.[30]

Gaussian functions were fitted to the 2θ-plot for each WAXS pattern to a confidence of at least 95%, using Matlab R2024b. The area of the most dominant peak at ≈20.6° was divided by the total of the detected area under the curve, to create a crystallinity index k according to eqn (4).

$$k = \frac{A_{20.6^\circ}}{A_{total}} \times 100\% \quad (4)$$

Mechanical characterisation

Tensile testing was performed on a Universal Testing System (Instron 5967, Illinois Tool Works Inc.) with a 30 kN load cell using a strain rate of 100% min^{-1}. Rectangular samples 60 mm × 10 mm × 0.5 mm ($L \times W \times D$) were cut from sheets, sealed inside a Teflon bag, heated to 200 °C and subsequently quenched in ice water prior to testing. Strain was determined from crosshead travel and clamp distance. A climate chamber (Instron 3119, Illinois Tool Works Inc.) was used to control the ambient temperature during testing.

Results and discussion

The aim of this work is to design a rubber-elastic polymer network that crystallizes only upon stretching and is inhibited against thermal crystallization. This self-reinforcement by strain-induced crystallization should allow the material for withstanding high loads at high elongation. In order to get an overview on the miscibility and thermal crystallization of the two polymers in mixture, blends of PVDF and PEtOx were prepared over the entire composition range and the maximum solubility of PVDF in PEtOx in dependence on cooling conditions was determined.

For this purpose, the crystallinity x_c and glass transition temperature T_g of the differently composed blends were determined by differential scanning calorimetry (DSC) in order to obtain information regarding their mixing behaviour in dependence on cooling conditions. All samples were cooled with a rate of 10 K min^{-1} as well as quenched from melt, respectively,

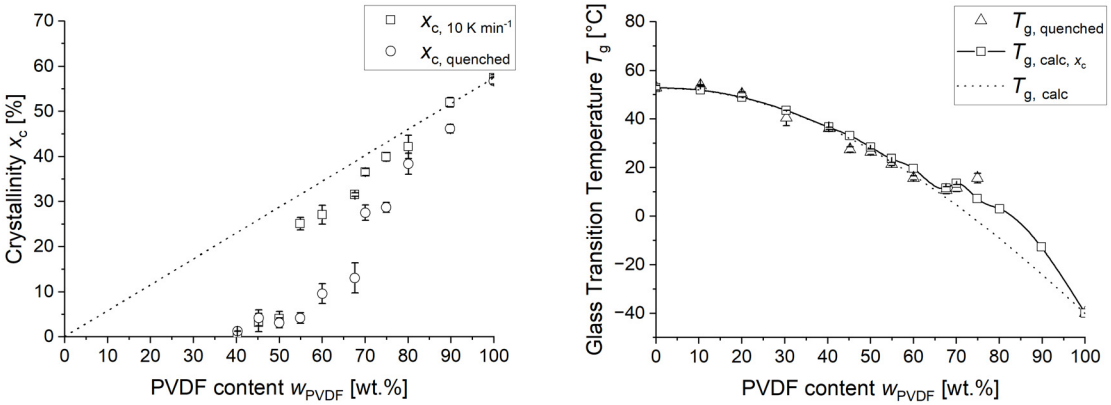

Fig. 1 (left) Crystallinity x_c of PVDF/PEtOx blends cooled from 200 °C in dependence on PVDF content and cooling condition (squares 10 K min^{-1}, circles quenched) in contrast to the calculated crystallinity (dashed line). (right) Measured glass transition temperatures $T_{g,blend}$ (Δ) of quenched PVDF/PEtOx blends in dependence on PVDF content in contrast to the calculated mixture glass transition temperature $T_{g,calc}$ (dotted line) assuming complete miscibility over the entire composition range. The squares with an interpolated solid line depict the crystallization-corrected calculated glass transition temperature ($T_{g,calc,x_c}$) of the remaining amorphous phase.

before they were subsequently reheated during the DSC measurement to 200 °C with 10 K min^{-1}.

Fig. 1 (left) shows the crystallinities of the differently composed blends determined after quenching as well as cooling with 10 K min^{-1}, respectively. Below approximately 40 wt% PVDF, no crystallinity is observed. Between 40 and 50 wt%, a minor fraction of less than 5 wt% of crystals were found independent on the cooling rate. A distinct influence of the cooling rate becomes evident above 55 wt% PVDF, where samples cooled at 10 K min^{-1} exhibit significantly higher crystallinity than the quenched samples. Above 65 wt% PVDF the crystallinity of the quenched samples approaches the calculated maximum crystallinity of the blends.

Fig. 1 (right) shows the measured glass transition temperatures ($T_{g,blend}$) together with the calculated mixture glass transition temperatures ($T_{g,calc,x_c}$) as a function of the PVDF content for the quenched PVDF/PEtOx blends. The dotted line represents $T_{g,calc}$ in dependence on PVDF content assuming complete miscibility over the entire composition range. Expectedly, the glass transition temperature of the amorphous phase increases, since the formation of crystals detracts PVDF from the surrounding amorphous phase. The glass transition temperature ($T_{g,calc,x_c}$) of the altered amorphous phase was derived from the PVDF crystallinity using eqn (3) and is depicted by the squares and an interpolated solid line in Fig. 1 (right).

The measured T_g corresponds well with $T_{g,calc}$ up to 65% PVDF for the quenched samples. Above these PVDF contents the measured $T_{g,quenched}$ deviates from the course of $T_{g,calc}$ to higher values. However, when considering the amount of PVDF crystals as the reduced content of this polymer in the amorphous blend, the values show a better fit. Thus, the higher degree of crystallinity is most likely causing a higher T_g in the blends at PVDF contents above 65%. This leads to the conclusion that quenching is not capable of increasing the maximum solubility of PVDF in PEtOx, which is between 30 and 40 wt% PVDF concentration. However, the formation of larger amounts of crystallinity can be effectively inhibited upon quenching up to a PVDF concentration of about 65 wt%.

Literature suggest that this might be due to a strongly increased melt viscosity along with the strong intermolecular interactions between PEtOx and PVDF.[31,32] This slows down mobility of the chains and thus separation of PVDF along with crystallization of the latter. A similar effect is known for PET as well.[33]

Next, PVDF/PEtOx networks were prepared over the entire composition range according to a previously published method[25] by dissolving the varying amounts of PVDF and PEtOx in dimethyl sulfoxide (DMSO), followed by the addition of dicumyl peroxide (DCP) and triallyl isocyanurate (TAIC). The mixtures were compression-moulded at 160 °C and cured at this temperature for 30 min.

Lowly and highly crosslinked PVDF/PEtOx networks, referred to as LC and HC, respectively, were prepared to investigate the influence of the extent of crosslinking on the maximum solubility and crystallization behaviour. In order to quantify the degree of crosslinking of LC- and HC-PVDF/PEtOx networks, representative compositions were analysed in a Dynamic Mechanical Analyzer (DMA) and the plateau modulus at 200 °C was utilised to calculate the netchain molecular weight according to eqn (1). The resulting netchain molecular weights are listed in Table 1.

Table 1 Netchain molecular weights of representative compositions of LC- and HC-PVDF/PEtOx blend networks

Composition	LC-PVDF/PEtOx	HC-PVDF/PEtOx
w_{PVDF} [wt%]	M_c [kg mol^{-1}]	M_c [kg mol^{-1}]
30	17.0	1.6
65	24.0	1.8

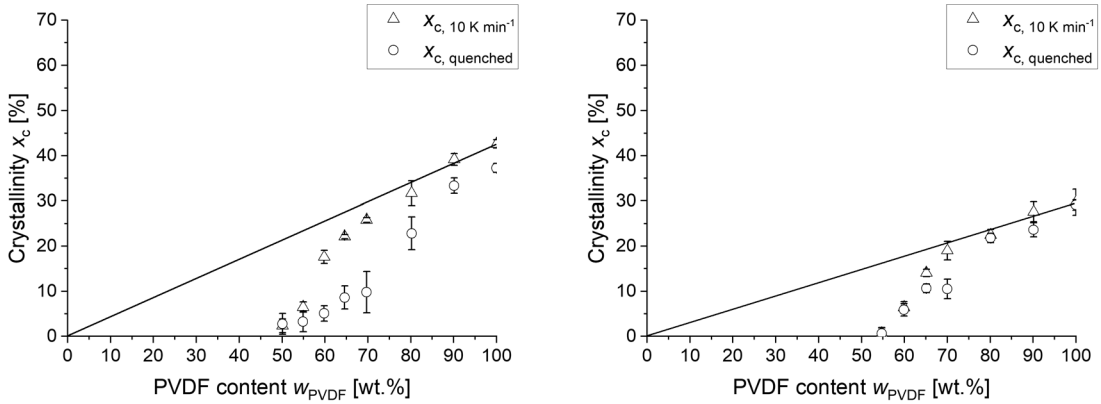

Fig. 2 Crystallinity x_c of differently crosslinked PVDF/PEtOx blends (left LC, right HC) determined directly after quenching and cooling with 10 K min^{-1}, respectively. The dotted line indicates the calculated maximum possible crystallinity of the blends.

All networks were quenched from the melt at 200 °C to 10 °C and immediately analysed with DSC between −40 °C and 200 °C using a temperature rate of 10 K min^{-1} to determine the dependence of crystallinity x_c on cooling conditions. Fig. 2 shows the determined x_c of the differently composed networks after cooling with 10 K min^{-1} and quenching, respectively. Similar to the blends, the cooling conditions have no effect on the maximum solubility of PVDF in PEtOx, evident by the unchanged crystallinity of the first composition, where crystals are formed. However, crosslinking shifts the onset of crystallization to significantly higher PVDF concentrations, being 50 wt% for the LC and 55 wt% for the HC samples. This finding suggests that crosslinking can increase the maximum solubility of PVDF in PEtOx. However, only the LC blends underwent efficient crystallization inhibition upon quenching. Fig. 3 depicts the glass transition temperature of the LC and HC blends after quenching from the melt. Up to 65 wt% PVDF, the quenched networks follow the prediction of T_g considering full miscibility. Above 65 wt% PVDF the measured glass transition temperature is significantly higher than the predicted ($T_{g,calc}$), which explains the fact that crystallization can no longer be inhibited in these networks. The lower crystallinity of the crosslinked samples is due to the fact that cross-linking point similar to branching points suppress crystal growth in polymers.

As seen in Fig. 2 and 3, the LC-PVDF/PEtOx network stays fully amorphous up to a PVDF content of 40 wt% and displays a mixed T_g of 30 °C. This obviously fully miscible composition was checked regarding the ability of LC-PVDF$_{40}$/PEtOx$_{60}$ to crystallize upon strain. The network was stretched at different temperatures above its glass transition temperature, but below the T_m of PVDF crystals. At a temperature of 60 °C the network becomes elastically deformable up to 100% strain. After releasing the stretching force, the sample retracted and fully recovered its original length. Thus, the stretched state cannot be stabilized by formed crystals. In order to check if any crystals are formed upon stretching, the samples were cooled to room temperature in the elongated state and analysed by WAXS (see Fig. S1, SI). Since no crystals could be detected, a strain-induced de-mixing and crystallizing does not take place in case of the fully miscible LC-PVDF$_{40}$/PEtOx$_{60}$.

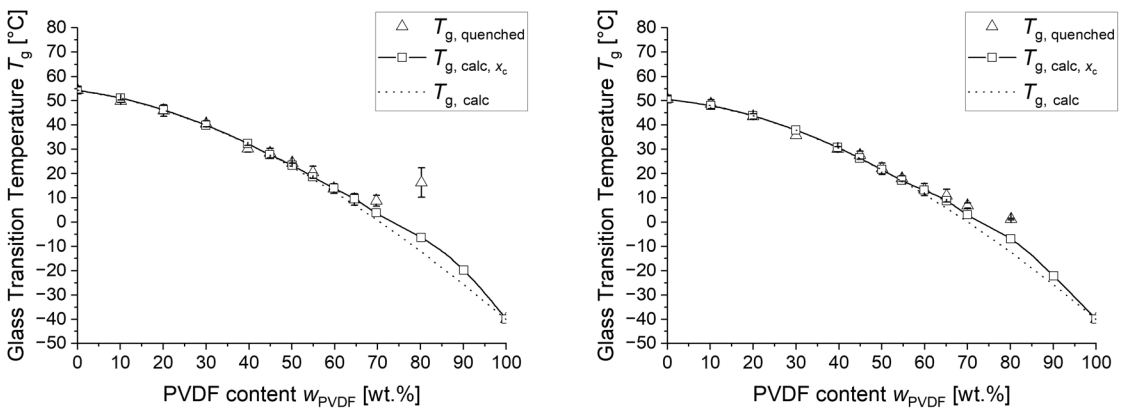

Fig. 3 Measured glass transition temperature T_g (triangles) of LC (left) and HC (right) crosslinked PVDF/PEtOx blends in dependence on composition and the calculated mixture glass transition temperature $T_{g,calc}$ (dotted line) assuming complete miscibility over the entire composition range. The squares with an interpolated solid line depict the crystallization-corrected calculated glass transition temperature ($T_{g,calc,x_c}$).

Thus, it was then investigated, if metastable LC-PVDF/PEtOx blends are capable of strain-induced crystallization. The most promising candidates are the LC samples with PVDF contents of 55, 60, and 65 wt%, because they possess a low crystallinity in quenched state, but have the potential to crystalize to higher degrees upon slow cooling as seen in Fig. 2 ($x_{c,quenched} < x_{c,10\ K\ min^{-1}}$). Further, these samples have a T_g below ambient temperature (20 °C). In order to test if the metastable LC-PVDF/PEtOx networks are self-reinforcing upon stretching by strain-induced crystallization, we decided to focus on the LC-PVDF$_{65}$/PEtOx$_{35}$ sample, because it has the lowest glass transition temperature (T_g) and inhibits the thermal crystallization to greatest extent. Thus, this network might also have the highest potential for strain-induced crystallization.

In order to determine whether these samples can self-reinforce by crystallizing under strain, rectangular samples were cut from sheets of the LC-PVDF$_{65}$/PEtOx$_{35}$ network. The samples were quenched and then immediately drawn in a tensile tester. Fig. 4 shows the stress–strain curves from representative samples drawn at RT, 30 °C and 50 °C.

The LC-PVDF$_{65}$/PEtOx$_{35}$ network drawn at room temperature as well as at a temperature of 30 °C shows a pronounced Hookean behaviour with a yield stress of up to 10 MPa followed by strain hardening up to a breaking stress of 41 MPa at a strain of 314% and 36 MPa at 285% strain, respectively. While this behaviour confirms the desired self-reinforcement due to strain-induced crystallization, the yield stress of 10 MPa contradicts previous expectations based on the measured mixture T_g well below room temperature. This increased stiffness at low elongation is most likely caused by either insufficient superheating of the amorphous phase above the glass transition temperature (T_g) or insufficient quenching resulting in a high degree of crystallinity, or a combination of both. To determine whether the higher yield stress is caused by crystals or the amorphous phase, a further sample was drawn at an increased temperature of 50 °C. This sample exhibited strain-hardening up to a breaking stress of 32.6 MPa at 405% strain, while showing a distinctly lower yield stress of about 2 MPa. As yield stress decreases upon drawing at 50 °C, the pronounced Hookean regime is likely caused by the stiffness of the amorphous phase itself rather than the crystals. WAXS patterns recorded immediately after quenching of the sample and subsequent drawing to an elongation of 400% at a temperature of 50 °C show an amorphous halo that alters upon drawing to a highly oriented semi-crystalline structure (see Fig. 4). The dominant peak at ≈20.6° indicates the strain-induced formation of *all-trans* β-PVDF crystals. In order to gain information whether and to which extent the T_g increase of the amorphous phase above ambient temperature or strain-induced crystals are responsible for stabilization of the material in the observed highly elongated shape after stretching, the recovery of LC-PVDF$_{65}$/PEtOx$_{35}$ strained to 400% at 50 °C immediately after quenching was recorded by DMA upon heating to 200 °C at a rate of 5 K min^{-1}.

The recovery *versus* temperature plot in Fig. 5 appears to display two separate mechanisms responsible for the recovery of the original shape – an initial recovery window between 30–50 °C corresponding to the glass transition temperature and a second recovery window between 60–170 °C corresponding to the melting of the strain induced crystals. The width of the second recovery window is most likely due to the broad nature of the crystallite size distribution.

Since the pronounced Hookean behaviour observed at room temperature and even 30 °C (see Fig. 4) do not seem to align with the glass transition temperature measured by DSC, we additionally determined the glass transition temperature from the mechanical relaxation measured by DMA.

As seen in Fig. 6, the T_g measured by DMA is 25 °C, which is significantly higher than the DSC-measured T_g of 9 °C. This explains the pronounced Hookean behaviour observed in the tensile tests at room temperature and 30 °C, as the samples are in the midst of their mechanical softening at this temperature. However, this still does not explain the large difference in

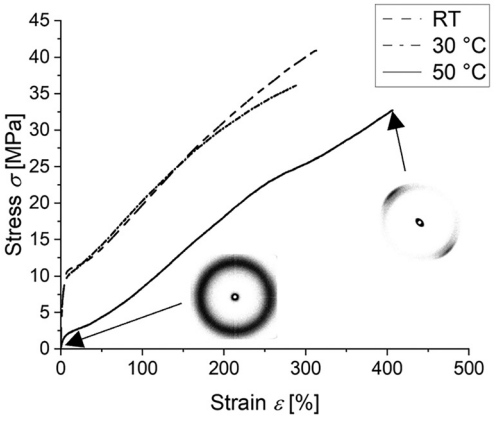

Fig. 4 Stress–strain diagrams of the LC-PVDF$_{65}$/PEtOx$_{35}$ sample immediately after quenching, drawn with a strain rate of 100% min^{-1} at room temperature, 30 °C and 50 °C, respectively. WAXS patterns of the quenched sample drawn at 50 °C are shown at strains of 0 and 400%, respectively.

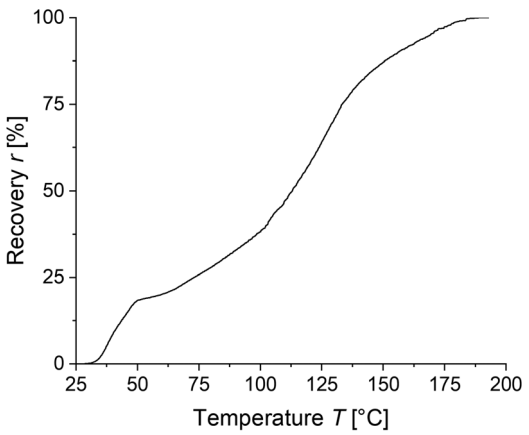

Fig. 5 Recovery *versus* temperature diagram of a quenched LC-PVDF$_{65}$/PEtOx$_{35}$ blend drawn to 400% at 50 °C.

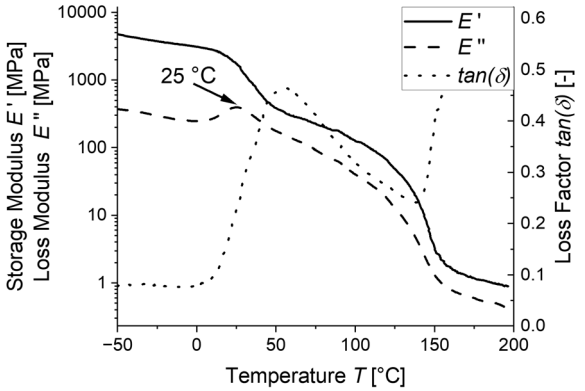

Fig. 6 DMA data of the LC-PVDF$_{65}$/PEtOx$_{35}$ network immediately after quenching. The T_g is determined at the maximum of the loss modulus.

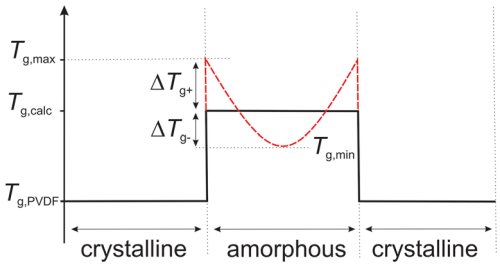

Fig. 8 Presumed T_g progression between PVDF crystals, caused by the crystallization-induced removal of PVDF from the amorphous phase in the vicinity of PVDF crystals.

the glass transition between the two measurement techniques. A potential reason for the difference in measurement might be caused by the crystals formed during quenching since the crystallization of PVDF leads to enrichment of PEtOx in the amorphous phase and potentially leaving behind an inhomogeneous amorphous phase. This inhomogeneity might not be detectable in the DSC evaluation. To increase the inhomogeneity and potentially allow it to be measured, we cooled the samples from 200 °C with a cooling rate of 10 K min^{-1} to allow crystallization and measured the glass transition in the DSC.

Fig. 7 shows the determined glass transition temperature of differently crosslinked PVDF/PEtOx blends after cooling with 10 K min^{-1}. The measured T_g corresponds to the calculated T_g of the ideal mixture and deviates not before significantly different crystallization between quenching and slowly cooling occurs. This is the case for samples with above 55 wt% PVDF for highly and 60 wt% PVDF for lowly crosslinked blends. Once such crystallization takes place the glass transition temperature increases not only above the ideal mixture glass transition temperature $T_{g,calc}$ but also above the crystallization corrected $T_{g,calc,x_c}$.

We suspect that the increased glass transition temperature above $T_{g,calc,x_c}$ is caused by the crystallization of PVDF leaving an inhomogeneous amorphous phase behind, which is unable to compensate the decreasing PVDF concentration in the immediate vicinity of the formed crystals and, thus, develops a high T_g region around the crystals. The suspected shape of the T_g progression between PVDF crystals is shown in Fig. 8.

If this holds true, this high T_g region should only be stable as long as the temperature remains below the measured T_g/$T_{g,max}$, or conversely, if the samples are annealed sufficiently long above T_g and below T_m, they should again form a more homogeneous mixture with the remaining amorphous phase. In order to proof this theory, we annealed the sample with the largest deviation from $T_{g,calc,x_c}$ – the LC-PVDF$_{65}$/PEtOx$_{35}$ sample – at a temperature of 80 °C for 24 h under exclusion of air and subsequently measured the T_g by DSC. Unfortunately, the higher crystallinity and the resulting lower portion of amorphous phase causes only a slight change in c_p, which does not allow any reliable statement to be made about a change in T_g. In order to confirm that according to our thesis

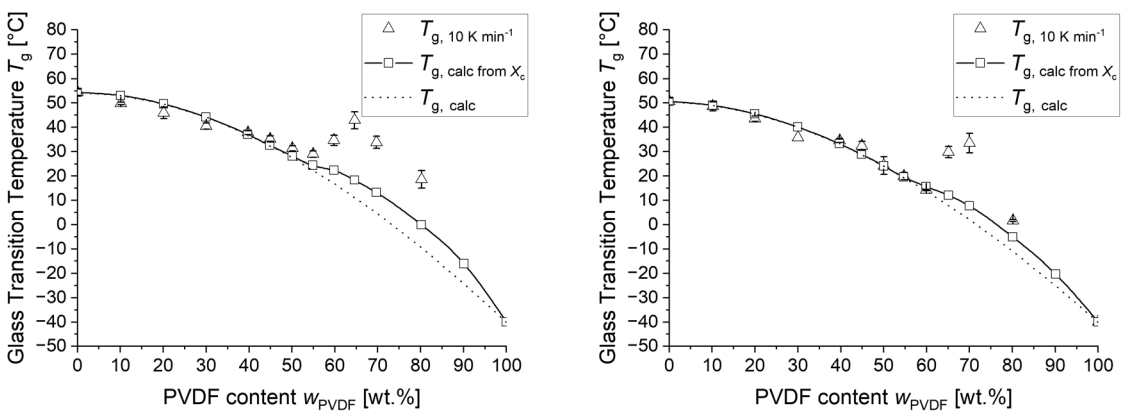

Fig. 7 Glass transition temperature T_g (triangles) of (left) LC and (right) HC PVDF/PEtOx blends in dependence on composition measured by DSC. The samples were cooled inside the DSC from 200 °C to −40 °C with 10 K min^{-1}. The calculated mixture glass transition temperature $T_{g,calc}$ (dotted line) is assuming complete miscibility over the entire composition range. The squares with an interpolated solid line depict the crystallization-corrected calculated glass transition temperature ($T_{g,calc,x_c}$).

the T_g decreases due to annealing, DMA measurements were carried out on LC-PVDF$_{65}$/PEtOx$_{35}$ samples directly after cooling from the melt with 10 K min^{-1} as well as after cooling with 10 K min^{-1} and subsequent annealing at 80 °C for 24 h. As shown in Fig. 9, the DMA measurements show a significant decrease of T_g after the annealing process. This confirms our thesis of the formation of a high-T_g boundary layer around the PVDF crystals, especially since an increase in T_g instead of a decrease would have to be expected due to the increasing crystallinity after annealing, resulting in even greater removal of PVDF from the amorphous phase.

The existence of a high-T_g boundary layer raises the question, if it is capable of acting as crystallization barrier that efficiently inhibits crystal growth of seed crystals at temperatures around and even above the calculated T_g of the remaining PVDF/PEtOx mixture in the amorphous phase. In order to answer this question, we performed WAXS experiments to monitor the crystal growth for different annealing temperatures above the crystallinity-corrected calculated mixture $T_{g,calc,x_c}$. To this end, the LC-PVDF$_{65}$/PEtOx$_{35}$ blend was measured immediately after quenching by wide angle X-ray scattering (WAXS) at different annealing temperatures. We chose the (200)-reflection of the PVDF β-crystals to calculate the crystallinity index k by deconvoluting the diffractogram and dividing the peak area of the (200) reflection by the total area of the diffractogram in the 2θ range from 7 to 22.3°.

Fig. 10 depicts the crystal growth of a quenched LC-PVDF$_{65}$/PEtOx$_{35}$ sample in dependence on annealing temperature, indicated by the crystallinity index k. As verified by DSC, carried out after an annealing time of 48 h, the maximum possible crystallinity forms, when the annealing temperature is 60 °C or above. The lower the annealing temperature below 60 °C, the less crystallinity is formed. This confirms our assumption that the significantly higher measured T_g compared to the calculated T_g is indeed related to the formation of a high-T_g boundary layer around the crystals, which inhibits thermal crystallization all the more effectively the lower the ambient temperature. It is noteworthy that the crystallization-induced separation of PVDF and PEtOx and the resulting formation of the high-T_g boundary inhibit thermal crystallization even far above the calculated mixture T_g.

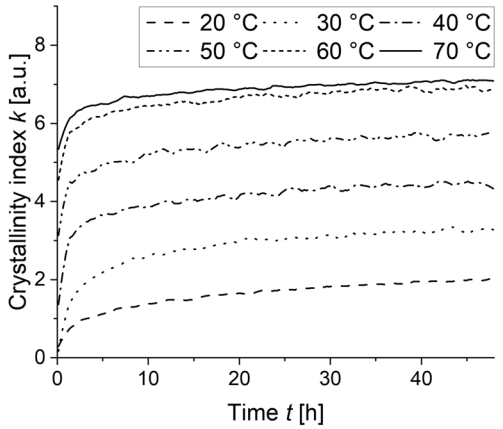

Fig. 10 Progress of crystallinity index k with time of a quenched, LC-PVDF$_{65}$/PEtOx$_{35}$ blend in dependence on isothermal annealing temperature.

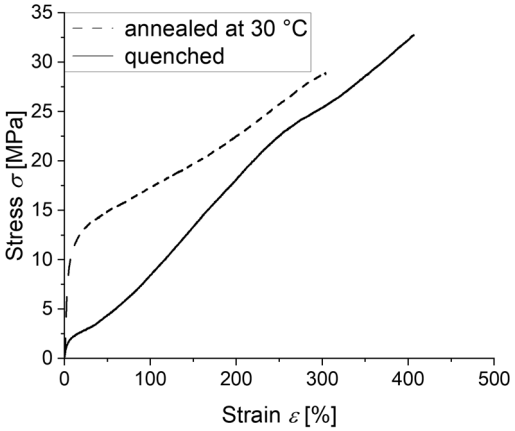

Fig. 11 Stress–strain diagrams of the LC-PVDF65/PEtOx35 blend, drawn at 50 °C directly after quenching (solid line) and after further storage at a temperature of 30 °C for 48 h (dotted line).

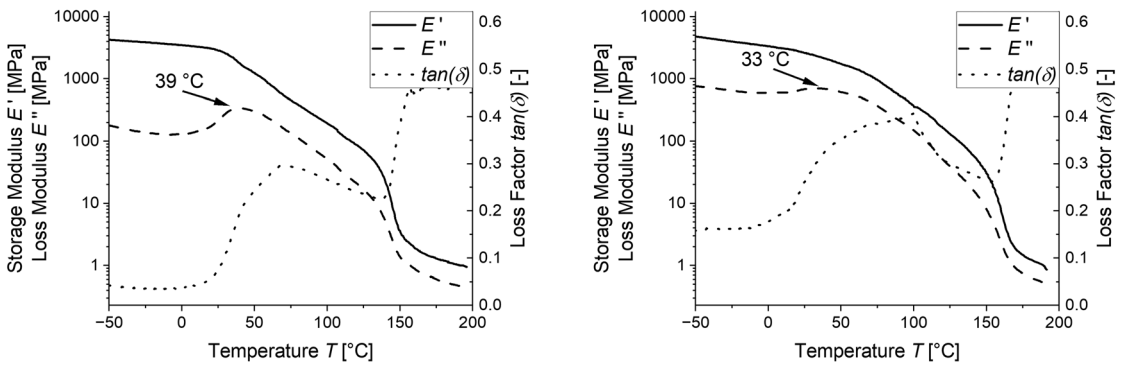

Fig. 9 DMA data of LC-PVDF65/PEtOx35 samples after cooling from 200 °C to room temperature with 10 K min^{-1} immediately (left) and after additional annealing at 80 °C for 24 h under exclusion of air (right), respectively. The T_g is determined at the maximum of the loss modulus.

In order to check whether a sample still self-reinforces due to strain-induced crystallization after prolonged storage at a temperature significantly above the calculated mixture T_g, stress–strain curves of the LC-PVDF$_{65}$/PEtOx$_{35}$ sample were recorded immediately after quenching and after storage for 48 hours at 30 °C, respectively. As seen in Fig. 11, although the yield stress increases due to the higher crystallinity after storage compared to the sample drawn directly after quenching, the ability to self-reinforce upon strain-induced crystallization is not lost.

Conclusions

The aim of this work was to design an amorphous, rubber-elastic polymer network made of PVDF and PEtOx that is inhibited against thermal crystallization but crystallizes when stretched and thus self-reinforces in a similar way to NR in order to withstand high loads at high elongation. To this end, we followed the novel strategy to crosslink a partially miscible blend of a semi-crystalline low-T_g and an amorphous high-T_g component that can be quenched into an amorphous rubber elastic state, when composed beyond the maximum solubility in the hope that it efficiently self-inhibits against thermal crystallization and crystallizes to a significant extent only upon stretching. It is shown at the example of a crosslinked blend of PVDF and PEtOx, that thermal crystallization truly self-inhibits but strain-induced crystallization still works and leads to self-reinforcement of this material. This is due to an effect that has not been observed before, whereby the formation of PVDF seed crystals in the quenched cross-linked blends pulls PVDF chains out of the surrounding amorphous phase, leading to an increase in T_g above ambient temperature in the immediate vicinity. This then prevents further crystallisation. This local phenomenon causes the desired self-inhibition of thermal crystallisation to work efficiently even above ambient temperature due to the formation of the high-T_g boundary layer around the crystals. While the blends described here are not yet suitable as rapid energy and shock absorbers, the findings are valuable for achieving such properties in similar alternative systems. Future studies will focus on investigating blends of PVDF and other carbonyl-containing polymers, particularly those with a lower T_g, to tailor them for use as RESA materials.

Author contributions

Robert D. L. Jerusalem: data curation, investigation, methodology, project administration, software, validation, visualization, writing – original draft, writing – review & editing. Michail Maricanov: validation, writing – review & editing. Anas Kerkour el Miad: investigation. Hannah Keune: investigation. Frank Katzenberg: supervision, writing – review & editing. Joerg C. Tiller: funding acquisition, project administration, supervision, writing – review & editing.

Conflicts of interest

There are no conflicts to declare.

Data availability

The data supporting this article have been included as part of the supplementary information (SI). Supplementary information: WAXS diffractogram of streched LC-PVDF$_{40}$/PEtOx$_{60}$ and compositions used for synthesizing PVDF/PEtOx blends as well as LC and HC networks. See DOI: https://doi.org/10.1039/d6lp00013d.

Acknowledgements

The authors acknowledge support from funding provided by the Deutsche Forschungsgemeinschaft DFG under grant TI 326/8-1 and INST 212/303-1 FUGG.

References

1 M. Behl and A. Lendlein, *Mater. Today*, 2007, **10**, 20–28.
2 R. Hoeher, T. Raidt, M. Rose, F. Katzenberg and J. C. Tiller, *J. Polym. Sci., Part B: Polym. Phys.*, 2013, **51**, 1033–1040.
3 T. Raidt, R. Hoeher, F. Katzenberg and J. C. Tiller, *Macromol. Rapid Commun.*, 2015, **36**, 744–749.
4 T. Raidt, R. Hoeher, M. Meuris, F. Katzenberg and J. C. Tiller, *Macromolecules*, 2016, **49**, 6918–6927.
5 D. Quitmann, N. Gushterov, G. Sadowski, F. Katzenberg and J. C. Tiller, *Adv. Mater.*, 2014, **26**, 3441–3444.
6 Y. Qiu, E. Askounis, F. Guan, Z. Peng, W. Xiao and Q. Pei, *ACS Appl. Polym. Mater.*, 2020, **2**, 2008–2015.
7 P. Awasthi and S. S. Banerjee, *Polymer*, 2022, **259**, 125338.
8 J. A. Jaber and J. B. Schlenoff, *J. Am. Chem. Soc.*, 2006, **128**, 2940–2947.
9 B. D. Johnson, D. J. Beebe and W. C. Crone, *Mater. Sci. Eng., C*, 2004, **24**, 575–581.
10 E. Verploegen, J. Soulages, M. Kozberg, T. Zhang, G. McKinley and P. Hammond, *Angew. Chem., Int. Ed.*, 2009, **48**, 3494–3498.
11 E. Samoylova, L. Ceseracciu, M. Allione, A. Diaspro, A. C. Barone and A. Athanassiou, *Appl. Phys. Lett.*, 2011, **99**, 201905.
12 S. Lee, Y. E. Cho, H.-Y. Kim and J.-Y. Sun, *Small*, 2025, **21**, 2412657.
13 J. Liu, Z. Tang, J. Huang, B. Guo and G. Huang, *Polymer*, 2016, **97**, 580–588.
14 C. R. López-Barrón, B. Rohde, A. V. Zabula, J. J. Schaefer and J. A. Throckmorton, *Macromolecules*, 2020, **53**, 1356–1367.
15 N. Candau, G. Stoclet, J.-F. Tahon, A. Demongeot, E. Yilgor, I. Yilgor, Y. Z. Menceloglu and O. Oguz, *Polymer*, 2021, **223**, 123708.

16 D. Quitmann, F. M. Reinders, B. Heuwers, F. Katzenberg and J. C. Tiller, *ACS Appl. Mater. Interfaces*, 2015, **7**, 1486–1490.
17 F. Katzenberg and J. C. Tiller, *J. Polym. Sci., Part B: Polym. Phys.*, 2016, **54**, 1381–1388.
18 T. Raidt, P. Santhirasegaran, R. Hoeher, J. C. Tiller and F. Katzenberg, *Macromol. Chem. Phys.*, 2019, **220**, 6.
19 K. Numata, H. Masunaga, T. Hikima, S. Sasaki, K. Sekiyama and M. Takata, *Soft Matter*, 2015, **11**, 6335–6342.
20 D. C. Wahrmund, R. E. Bernstein, J. W. Barlow and D. R. Paul, *Polym. Eng. Sci.*, 1978, **18**, 677–682.
21 D. R. Paul, J. W. Barlow, R. E. Bernstein and D. C. Wahrmund, *Polym. Eng. Sci.*, 1978, **18**, 1225–1234.
22 R. E. Bernstein, D. C. Wahrmund, J. W. Barlow and D. R. Paul, *Polym. Eng. Sci.*, 1978, **18**, 1220–1224.
23 R. E. Bernstein, D. R. Paul and J. W. Barlow, *Polym. Eng. Sci.*, 1978, **18**, 683–686.
24 J. Schaup and F. Katzenberg, Abstr. Pap. Am. Chem. Soc., 2010, **239**, 1.
25 R. D. L. Jerusalem, M. Maricanov, F. Katzenberg and J. C. Tiller, *ACS Appl. Polym. Mater.*, 2025, **7**, 932–937.
26 K. Nakagawa and Y. Ishida, *Kolloid Z. Z. Polym.*, 1973, **251**, 103–107.
27 D. Segiet, T. Raidt, H. Ozdem, S. Weckes, J. C. Tiller and F. Katzenberg, *J. Polym. Sci., Part B: Polym. Phys.*, 2019, **57**, 1053–1061.
28 R. E. Belke and I. Cabasso, *Polymer*, 1988, **29**, 1831–1842.
29 L. A. Utracki, *Polymer alloys and blends: thermodynamics and rheology*, Hanser, Munich u.a., 1989.
30 R. Hasegawa, Y. Takahashi, Y. Chatani and H. Tadokoro, *Polym. J.*, 1972, **3**, 600–610.
31 L. Mandelkern, *Chem. Rev.*, 1956, **56**, 903–958.
32 H.-H. Yang, C. D. Han and J. K. Kim, *Polymer*, 1994, **35**, 1503–1511.
33 R. D. L. Jerusalem, M. Maricanov, T. Raidt, F. Katzenberg and J. C. Tiller, *Macromol. Rapid Commun.*, 2024, **45**, 2400346.